*Materials Research.* 2017; 20(3): 619-627
DOI: http://dx.doi.org/10.1590/1980-5373-MR-2016-0569


# Synthesis of Surface Oxygen-deficient $BiPO_4$ Nanocubes with Enhanced Visible Light Induced Photocatalytic Activity

***Bingtao Shi[a], Haoyong Yin[a]*, Tao Li[a], Jianying Gong[a], Shumei Lv[a], Qiulin Nie[a]***

[a] *College of Materials & Environmental Engineering, Hangzhou Dianzi University, Hangzhou, 310018, P. R. China*

Received: August 05, 2016; Revised: January 19, 2017; Accepted: February 18, 2017

The visible light driven $BiPO_4$ nanocubes with sufficient surface oxygen deficiency were fabricated by a hydrothermal process and subsequently ultrasonic assistant Fe reduction process. The products were characterized by XRD, DRS, XPS, SEM and TEM which showed that the $BiPO_4$ had cuboid-like shape with a smooth surface and clear edges and the oxygen vacancies were succesfully introduced on the surface of the $BiPO_4$ nanocubes. The as prepared oxygen-deficient $BiPO_4$ nanocubes showed greatly enhanced visible light induced photocatalytic activity in degradation of Rhodamine B. The enhanced photocatalytic performance and expanded visible light response of $BiPO_4$ may be due to the introduction of surface oxygen vacancies which can generate the oxygen vacancies mid-gap states lower to the conduction band of $BiPO_4$.

**Keywords:** *$BiPO_4$; Nanocubes; Photocatalysis; Oxygen vacancy*

## 1. Introduction

Photocatalysis has attracted considerable attention ever since the photocatalytic splitting of water on $TiO_2$ electrodes was investigated by Fujishima and Honda[1], which provides a new promising way to meet the challenges of the environment, energy and sustainability with abundant solar light[2-4]. Although $TiO_2$ is the most promising photocatalyst and is widely investigated due to its non-toxicity, chemical stability and low cost, low solar energy conversion efficiency and high recombination of photogenerated electron-hole pairs make it difficult for practical applications[5,6]. Therefore, it is necessary to fabricate efficient new types of photocatalysts capable of responding to visible light in order to improve the utilization of solar energy.

As is known that visible light response of the photocatalyst needs the narrow band gap in the semiconductors. However, the highly photocatalytic efficiency always requires the higher valence band (VB) and lower conduction band (CB) of the semiconductor photocatalyst, which can provide enough oxidation and reduction power of the holes and electrons respectively[7,8]. The discrepancy always makes the highly photocatalytic efficient photocatalyst less visible light response. For instance, $BiPO_4$, with a novel nonmetal oxy-acid salt structure, has the suitable VB and CB position for highly photocatalytic performance which showed twice higher activity than that of $TiO_2$ (P25, Degussa) for the degradation of organic dye under UV light[9]. However, the large band gap energy of $BiPO_4$ (3.85 eV) prevented it from utilizing the visible light to meet the requirement of practical application[10,11]. Therefore, great efforts have been made to broaden the visible light absorption region and obtain high visible light induced photocatalytic performance of $BiPO_4$. As is known coupling of a narrow band gap semiconductor such as CdS[12], BiOI[13] and $Ag_3PO_4$[14] on the $BiPO_4$ surface to form the p-n heterojunctions can increase the visible light induced photocatalytic activities of the catalyst. However, the charge separation in this p-n heterojunctions always undergoes the photogenerated electrons transferring to the CB of $BiPO_4$ leaving holes on the VB of narrow band semiconductors[12-14], which can hardly use the high oxidation ability of holes in the higher VB of $BiPO_4$. Recently, the oxygen defects have been reported can greatly enhance the photocatalytic activity and expand the range of photoresponse in the semiconductor photocatalysts[15-18]. As investigated, the oxygen vacancies can not only serve as photoinduced charge traps to prevent the electron−hole recombination, they are also effective adsorption sites to adsorb active species which may greatly increase the photocatalytic activity[17,18]. Moreover, oxygen vacancies can also form oxygen vacancy states lying close to the conduction band of the photocatalyst, which can enhance its visible light response[17]. Except for $TiO_2$ and BiOCl, Zhu et al.[18,19] also reported that oxygen vacancies enriched $BiPO_4$ nanorod, prepared by vacuum deoxidation, showed enhanced photocatalytic activity and expanded photocatalytic response (more than 365 nm). However, the investigation of the oxygen-deficient $BiPO_4$ is still insufficiency and the interior mechanism and some details of the visible light induced photocatalysis are yet not very clear. Therefore, it is still necessary to develop oxygen-deficient $BiPO_4$ with different morphology using more facile and milder process and further investigate the interior mechanism of oxygen vacancies effect on the photocatalytic activity.

* e-mail: yhy@hdu.edu.cn

In this work, we reported a facile method to prepare the oxygen-deficient $BiPO_4$ nanocubes through an ultrasonic assistant Fe reduction process. The $BiPO_4$ nanocubes were firstly synthesized by a hydrothermal process and then surface oxygen vacancies were generated by ultrasonic assistant Fe reduction process. The oxygen-deficient $BiPO_4$ nanocubes showed greatly enhanced visible light induced photocatalytic activity. The organic pollutant was mainly photodegraded by •OH and holes in the VB of $BiPO_4$, which may be due to the visible light induced electron and holes separation originated from oxygen vacancy states.

## 2. Experimental

### *2.1 Preparation of the $BiPO_4$ nanocubes*

In a typical procedure, 5mmol bismuth nitrate ($Bi(NO_3)_3 \cdot 5H_2O$) and 5mmol ethylenediamine tetraaceticacid disodium salt (EDTA) was added to 100 ml distilled water under magnetic stirred at ambient temperature. Then the nirtic acid ($HNO_3$, 1.8ml) was slowly added dropwisely into the solution. Until the precursor solution became transparent, 5 mmol potassium monophate ($K_2HPO_4$) was then added and continuously stirred magnetically for 10 min. The resulting precursor suspension was transferred into a Teflon-lined stainless steel autoclaveand maintained at 180 ºC for 12h. The product was then separated by centrifugation and washed by distilled water and ethanol for several times. Finallly, the $BiPO_4$ nanocubes were obtained after the products dried at 70 ºC for 12h which were denoted as $WBiPO_4$.

### *2.2 Preparation of the oxygen-deficient $BiPO_4$ nanocubes*

As prepared $BiPO_4$ nanocubes (0.6g) and reduced iron powder (0.6g) were directly dispersed in 40ml distilled water at ambient temperature. The mixture was mechanically stirred and kept under ultrasonic for 5h (power of ultrasonication was 800W). After reduction, the yellow samples and excess Fe powder were separated by an external strong magnetic field, and then the sample was maintained in dilute hydrochloric acid (0.01M) for 30min in order to fully remove the Fe powder residue. The product was collected and washed with absolute alcohol and deionized water for several times and finally dried at 70 ºC for 12h. The oxygen-deficient $BiPO_4$ nanocubes were denoted as $GBiPO_4$.

### *2.3 Characterization*

The morphologies and microstructures of the photocatalysts were characterized using scanning electron microscope (SEM, Hitachi S-4700) and transmission electron microscopy (TEM, JEOL 200CX). X-ray diffraction (XRD, Thermo ARL SCINTAG X'TRA) was used to characterize the phase structures of the samples. UV-vis diffuse reflectance spectra were obtained on UV-vis spectrophotometer (UV-Vis, Shimadzu UV-2550) with $BaSO_4$ as reference. X-ray photoelectron spectroscopy (XPS) measurements were carried out on a PHI-5400 spectrometer using the C1s level at 284.6 eV as an internal standard to correct the shift of binding energy. The conventional three-electrode system was used to measure the photocurrent and electrochemical impedance spectroscopy (EIS) on an electrochemical workstation (Zennium, Zahner, Germany). FTO glass coated with the as-prepared samples (0.1 mg) served as the working electrode. The counter and the reference electrodes were a platinum plate and a saturated Ag-AgCl electrode, respectively. NaOH aqueous solution (0.1 M) was used as electrolyte. The working electrode (the active area 0.5 cm × 0.5 cm.) was prepared using an amended doctor blade method. Firstly 0.1 g of sample was ground with 1 mL terpineol. The slurry was then coated onto FTO glass by the doctor blade method which was cleaned in distilled water and ethanol by ultrasonication. These electrodes were preliminarily dried at 70°C and calcinated at 200°C for 1 h under Ar atmosphere.

### *2.4. Evaluation of the photocatalytic performance*

The photocatalytic performance of oxygen-deficient $BiPO_4$ nanocubes was evaluated by the degradation of Rhodamin B (RhB) solution under visible light irradiation. The light source was obtained by a 300W Xe lamp with a 420 nm cut off filter used to get the visible light. In each experiment, 0.1 g of the as-prepared photocatalyst was added into 100 mL of RhB solution (5mg/L). The well dispersed suspension was magnetically stirred in the dark condition for 30min to reach the adsorption/desorption equilibrium. After irradiation, about 5 mL of suspension was sampled at every interval and centrifuged to remove the photocatalysts. The concentration of filtrates was analyzed by measuring the maximum absorbance at 554 nm for RhB using a UV-2550 UV-vis spectrophotometer.

## 3. Results and Discussion

The morphologies of oxygen-deficient $BiPO_4$ nanocubes ($GBiPO_4$) and unreduced $BiPO_4$ ($WBiOP_4$) are firstly observed by SEM. Figure 1 shows SEM images of $WBiPO_4$ and $GBiPO_4$. It is clearly seen that the as synthesized $WBiPO_4$ had a cuboid-like shape with a smooth surface and clear edges (Figure 1a). The enlarged SEM image (Figure 1b) shows that the width of the nanocubes ranging from 400-800nm and length is about 600nm-1μm. Moreover, the cuboid-like crystal with a different facet was also observed on the enlarged SEM image. Figure 1c shows the SEM image of $GBiPO_4$ which displays the similar morphology of $WBiPO_4$ suggesting the reduction of $BiPO_4$ by Fe did not evidently change the morphologies of the photocatalyst. The

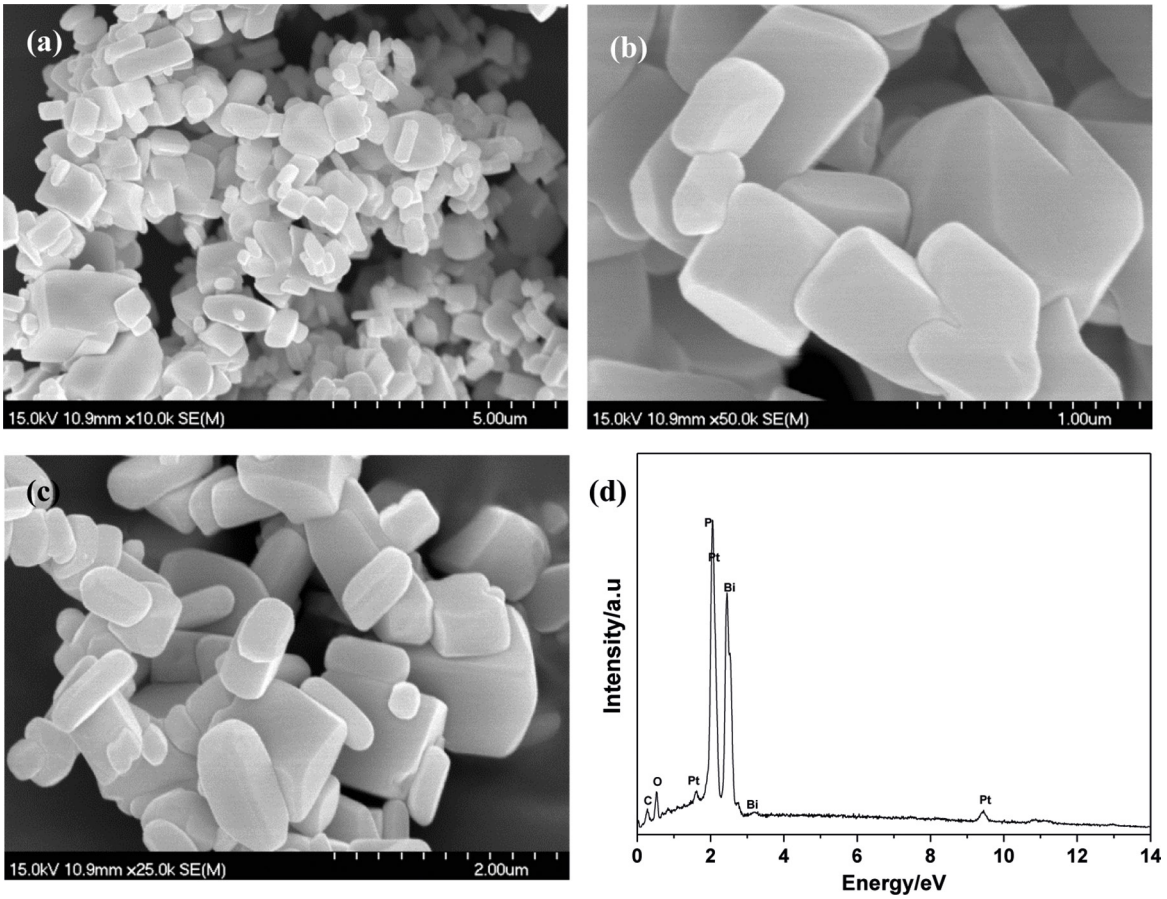


**Figure 1.** SEM images of (a), (b) $WBiPO_4$ and (c) $GBiPO_4$. (d) EDS analysis of $GBiPO_4$.

chemical composition of $WBiPO_4$ was confirmed by energy dispersive X-ray analysis (Figure 1d) which shows that Bi, O, P are major elements (except for the elements Pt and C from the Pt coating and conducting wafer used in SEM analysis respectively). No other impurities were found in the samples suggesting the relatively pure $BiPO_4$ can been obtained by this process.

TEM and HRTEM images were further demonstrated to observe the fine structure of $WBiPO_4$ and $GBiPO_4$ and the results were shown in Figure 2. TEM images of $WBiPO_4$ (Figure 2a) and $GBiPO_4$ (Insert of C) show the similar cuboid-like shape which is in consistent with the results of SEM analysis. Moreover, the evidently morphologies change for the two photocatalysts was still undetectable on the TEM images. On the HRTEM images of both $WBiPO_4$ (Figure 2b) and $GBiPO_4$ (Figure 2c) the distinct lattice spacing of about 0.196 nm can be clearly investigated which is consistent with the (212) crystallographic plane of $BiPO_4$[20]. Further investigation reveals that unreduced $BiPO_4$ displays perfect lattice features, however the edge of oxygen-deficient $BiPO_4$ becomes dim and disordered, which indicates that the surface structure of oxygen-deficient $BiPO_4$ is damaged and surface oxygen vacancies are formed. Similar phenomena has also been investigated in the previous research[19].

The XRD pattern was used to investigate the phase structures of the samples, and the typical diffraction patterns are shown in Figure 2d. It can be observed that the same XRD patterns were obtained on both $WBiPO_4$ and $GBiPO_4$, which could be indexed to the pure monoclinic phase of well-crystallized BiPO4, well consistent with the reported data (JPCDS 80-0209). The peaks at 2θ values of 19.01°, 21.31°, 27.13°, 29.04°, and 31.16° are corresponding to the diffraction peaks of (011), ($\bar{1}$11), (200), (120), and (012) crystal planes of $BiPO_4$, respectively. The similar XRD patterns suggested that the Fe reduction of $BiPO_4$ did not change the crystal phase of the photocatalyst. Moreover, there is no any trace of impurity phase detected, indicating the high purity and high crystallinity of the samples.

The XPS analysis was further carried out to analyze the chemical composition and elucidate the chemical state of the element in the oxygen-deficient $BiPO_4$ (Figure 3). The XPS survey spectrum (Figure 3a) clearly indicates that the $WBiPO_4$ was mainly composed of elements Bi, P and O (the C 1s peak at 284.8 eV may originate from adventitious hydrocarbon in the XPS instrument). A broad signal peak at about 132.7 eV in the high resolution XPS spectra of P (Figure 3b) suggests that the P in the sample exists in the oxidation state of $P^{5+}$. The peak in the high resolution XPS spectra of

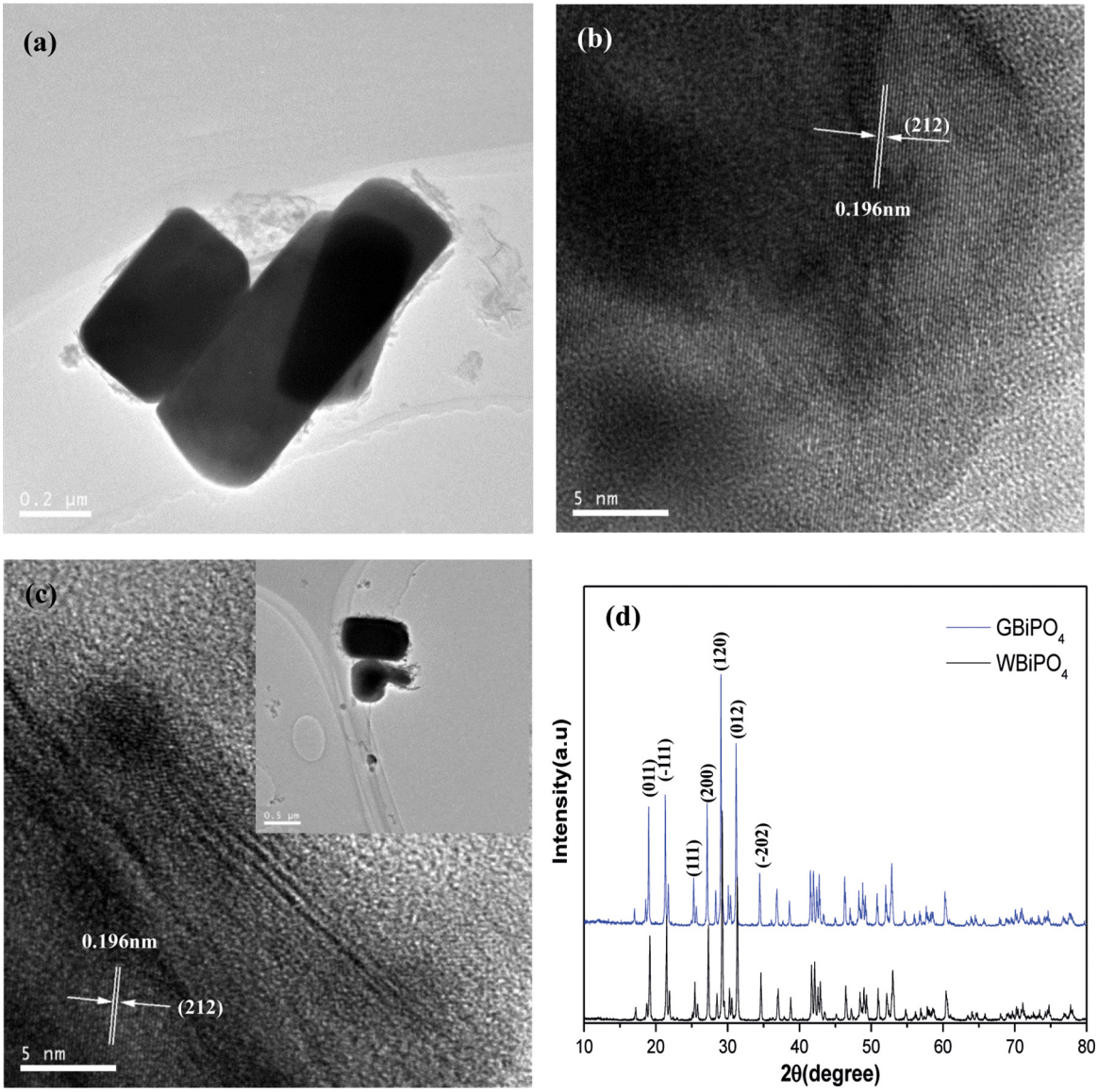


**Figure 2.** (a) TEM and (b) HRTEM images of $WBiPO_4$. (c) HRTEM images of $GBiPO_4$. (d) XRD patterns of $WBiPO_4$ and $GBiPO_4$. (Insert in C is the TEM image of $GBiPO_4$)

O (Figure 3c) locates at 531.2eV which can be attributed to O1s in $BiPO_4$. In the high resolution XPS spectrum of Bi (Figure 3d), the peak can be deconvoluted into two pair separate peaks. The peaks at 165.8 eV and 160.5 eV are indexed as $Bi^{3+}$ in $BiPO_4$. The lower binding energies at 163.3 eV and 158.2 eV can be indexed to lower charged Bi ions which are due to the oxygen vacancies present[17,21]. The same phenomenon has also occurred in other oxygen vacancies enriched BiOCl and $TiO_2$ systems, namely, the appearance of oxygen vacancies induced a lower binding energy peak which was due to $Bi^{3-x}$ or $Ti^{3+}$ [22-24].For comparison the high resolution XPS spectrum of Bi in $WBiPO_4$ has also been showed in Figure 3d. It can be seen that the peak is more symmetrical than that of $GBiPO_4$ which may indicate that there is no lower valence state Bi in $WBiPO_4$.

The structure of $WBiPO_4$ and $GBiPO_4$ was also further characterized by Raman spectroscopy as shown in Figure 4. In all spectra, the observed intense band at 165 $cm^{-1}$ with a shoulder at 231 $cm^{-1}$ corresponds to the Bi O stretching vibration. The bands centered at 1033 and 964 $cm^{-1}$ are ascribed to the asymmetric ($\nu_3$) and symmetric ($\nu_1$) stretching vibrations of the $PO_4$ group, respectively. The $\nu_4$ bending vibration modes of $PO_4$ groups occur at 554 and 596 $cm^{-1}$, and $\nu_2$ bending vibration occur at 403 and 458 $cm^{-1}$. It can be seen that although the positions of these Raman peaks were not changed but the intensities were decreased on $GBiPO_4$ which may be attributed to the contribution of oxygen vacancies[25].To further confirm the existence of oxygen vacancies the electron paramagnetic resonance (EPR) of $WBiPO_4$ and $GBiPO_4$ was also performed. As

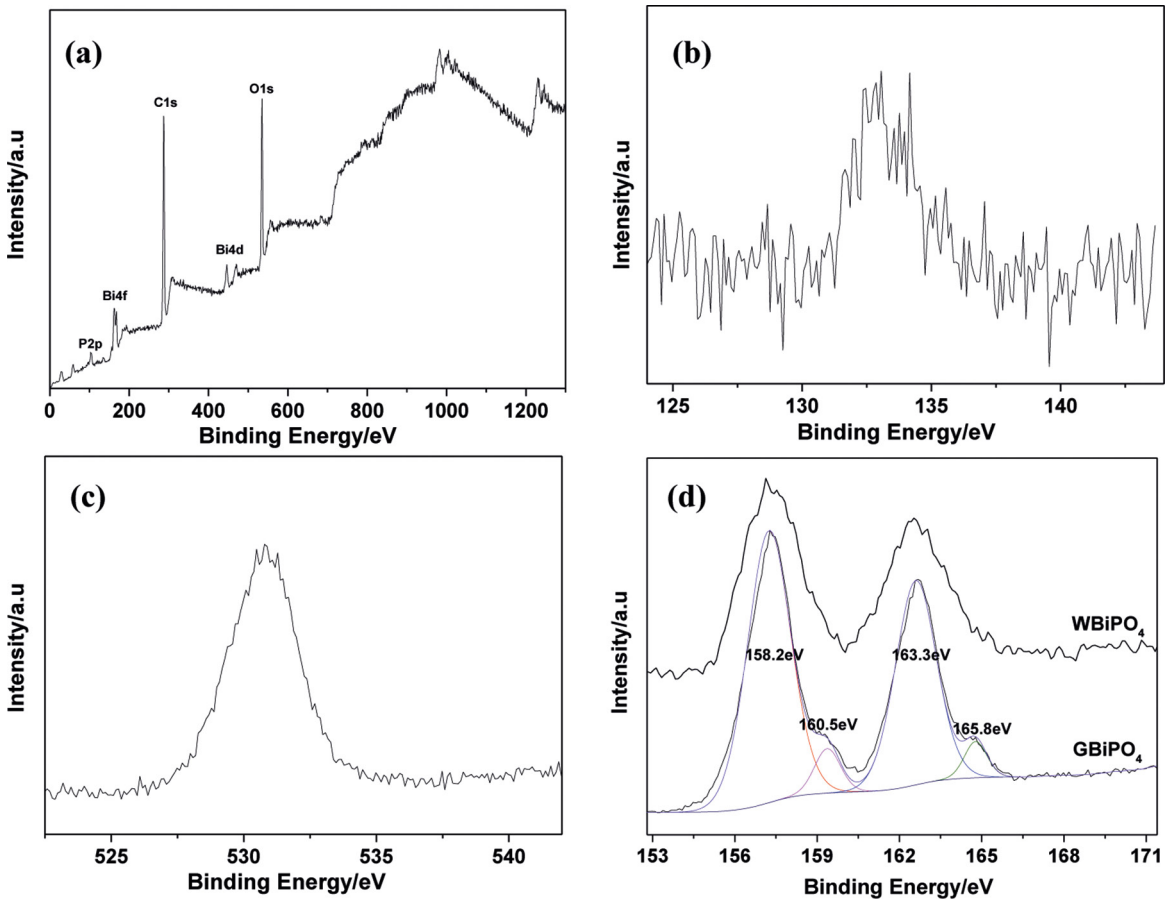


**Figure 3.** XPS profiles of $GBiPO_4$. (a) survey scan, (b) P2p core levels, (c) O1s core levels, (d) Bi4f core levels.

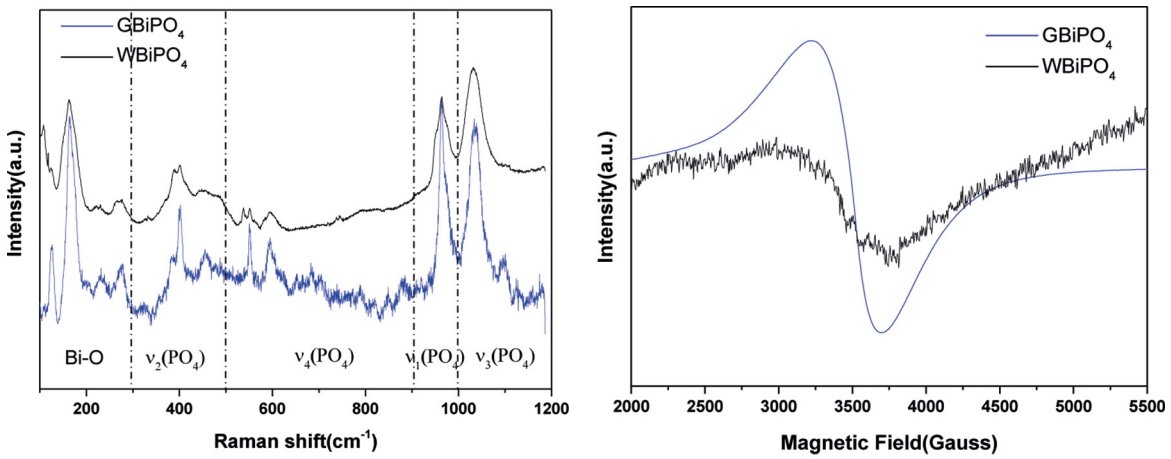


**Figure 4.** Raman spectrum (a) and EPR spectra (b) of $WBiPO_4$ and $GBiPO_4$.

investigated from Figure 4b the intensity of the EPR signal at $g \sim 2.001$ of $GBiPO_4$ is much higher than that of $WBiPO_4$ under the same conditions. As reported previously, g equal to $2.003 \pm 0.001$ can be attributed to oxygen vacancies on the surface[18,19,25] indicating that surface oxygen vacancies were produced on $GBiPO_4$.

It is well known that the light absorption and the migration of the light-induced electrons and holes are the key factors in determining photocatalytic activity, which rely on the electronic structure characteristics of the material. Diffuse reflectance spectroscopy (DRS) is a useful tool for characterizing electronic states in optical materials. Figure 5 displays the

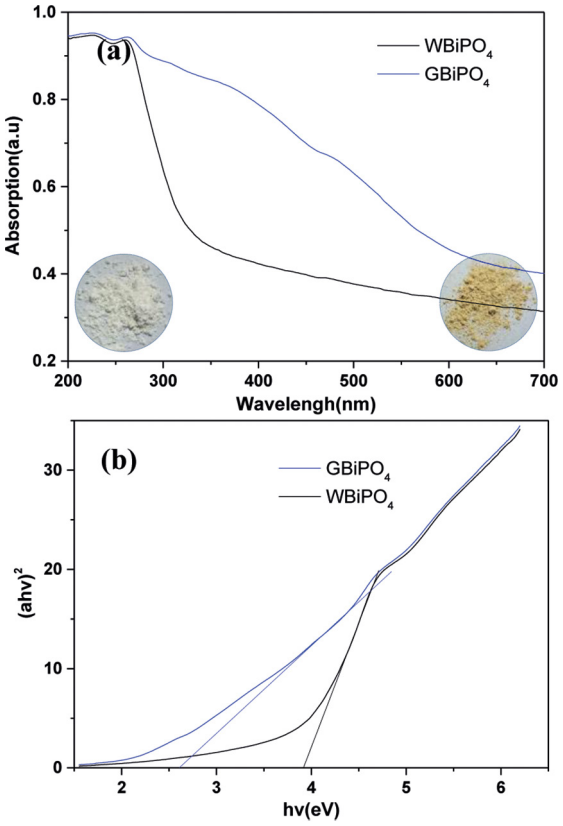


**Figure 5.** UV-vis diffuse reflectance spectra (a) and Band gap calculation by Tauc's method (b) of $WBiPO_4$ and $GBiPO_4$.

diffuse reflectance spectroscopy spectra of $WBiPO_4$ and $GBiPO_4$. It can be seen that $WBiPO_4$ only can absorb UV light due to its large bandgap energy. Moreover, the DRS of $GBiPO_4$ presents distinctly red shift with the increased absorption in the visible light region, which is probably due to the oxygen vacancies in the oxygen-deficient $BiPO_4$ [18,19]. From the inset of Figure 5A, the color of the as-prepared photocatalysts changed from white $WBiPO_4$ to light-yellow oxygen-deficient $GBiPO_4$, which is caused by the formation of oxygen vacancies. As a crystalline semiconductor, the estimated value of the band gap (Eg) of the samples could be calculated by the following formula:[20]

$$A(hv - Eg)^{n/2} = ahv \qquad (1)$$

where A, a, v, and Eg are the constant, absorption coefficient, light frequency, and band gap energy, respectively. In addition, n is determined by the type of optical transition of a semiconductor (n = 1 for a direct transition and n = 4 for an indirect transition). As $BiPO_4$ exhibits the characteristic of indirect band transition[26], the value of n is 4. The corresponding Eg values of $WBiPO_4$ and $GBiPO_4$ were determined from a plot of $(ahv)^2$ versus energy (hv) (Figure. 4b) and estimated to be 3.92 and 2.62 eV, respectively, which implied that $GBiPO_4$ nanocubes may have the best visible light induced photocatalytic activities.

The photocatalytic degradation of RhB by $WBiPO_4$ and $GBiPO_4$ was investigated, and the removal efficiencies as a function of reaction time are shown in Figure 6. As can be investigated in Figure 6a, RhB is degraded slightly under visible light illumination in the absence of photocatalysts, suggesting that the photolysis of RhB is negligible. Moreover, the photocatalytic activities of $WBiPO_4$ was also very low under visible light irradiation indicating no visible light photocatalytic activity of pure $BiPO_4$. In contrast, $GBiPO_4$ presented much higher photocatalytic activity for RhB degradation under the same conditions. The linear relationship between $\ln(C_0/C)$ and t shown in Figure 6b confirms that the photocatalytic degradation process of RhB followed the apparent pseudo-first-order model expressed in Eq. (2):

$$\ln(C_0/C) = kappt \qquad (2)^{27}$$

Where $C_0$ and Ct are the RhB initial equilibrium concentration and reaction concentration at time (t), and kappt is the reaction rate constant ($min^{-1}$). Thus, the kapps of $WBiPO_4$ and $GBiPO_4$ were calculated to be 0.000835, 0.00962 $min^{-1}$ respectively. The much higher rate constants indicated the oxygen-deficient $BiPO_4$ nanocubes had much stronger visible light induced photocatalytic activities than that of pure $BiPO_4$, which may be due to the oxygen vacancies induced enhancement of the visible light absorption and charge separation.

Photocurrent is an effective method to reflect the generation, separation and migration efficiency of photogenerated carriers and the photocurrent of $WBiPO_4$ and $GBiPO_4$ were recorded for several on-off cycles with a pulse of 40 s under visible light irradiation ($\lambda$> 420 nm). It can be seen from Figure 7a that the photocurrent appeared promptly when the samples were irradiated, indicating the generation of photogenerated electrons, and then decreased sharply as soon as the irradiation of light was turned off. In comparison with pure $BiPO_4$, the oxygen-deficient $BiPO_4$ nanocubes exhibits an obvious increased current density(The slight photocurrent response of pure $BiPO_4$ may arise from a small quantity of unfiltered UV light). In general, the value of the photocurrent indirectly reflects the ability in generation and transfer of the photoexcited charge carrier under irradiation. The higher photocurrent demonstrates the higher electrons and holes separation efficiency[13]. Therefore, the result of the photocurrent measurement may suggest that the oxygen-deficient $BiPO_4$ nanocubes have stronger ability in separation of electron–hole pairs than pure $BiPO_4$ which is consistent with the results of the visible light photocatalytic activities. Electrochemical impedance spectra (EIS) measurements were also conducted to investigate the charge transfer resistance and the separation efficiency of $WBiPO_4$ and $GBiPO_4$. As can be investigated in Figure 7b,

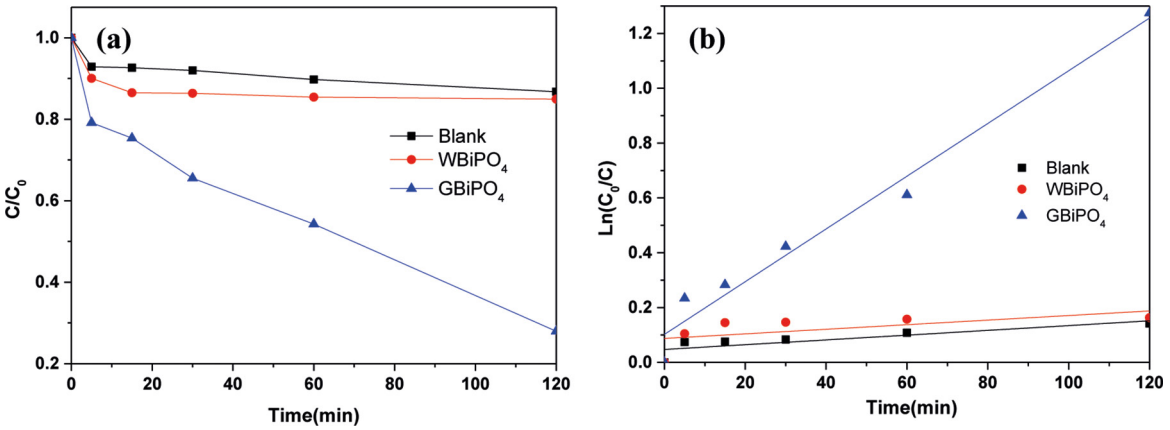


**Figure 6.** Photocatalytic degradation of rhodamine B (a) and plots of $\ln(C_0/C)$ versus time (b) with $WBiPO_4$ and $GBiPO_4$ under visible light irradiation.

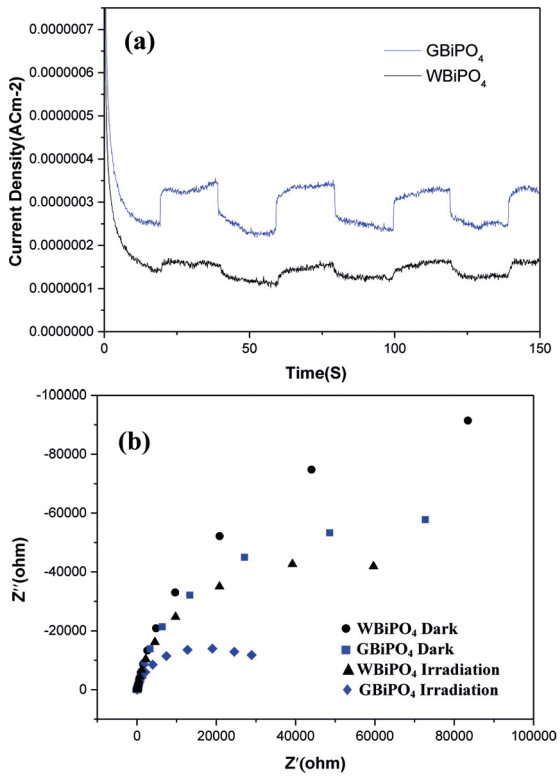


**Figure 7.** Comparison of (a) transient photocurrent response and (b) EIS Nyquist plots of $WBiPO_4$ and $GBiPO_4$.

the EIS Nyquist plots of $WBiPO_4$ and $GBiPO_4$ displayed similar impedance spectra, being composed of semicircle. However, compared with the $WBiPO_4$ and $GBiPO_4$, the arc radius of $GBiPO_4$ was smaller than that of $WBiPO_4$. As is known that a smaller impedance arc radius in Nyquist plots always indicates better electron-hole pair separation efficiency of the photocatalysts[28]. Therefore, the EIS results may also suggest that a more effective separation of photogenerated electron-hole pairs and faster interfacial charge transfer occurred on the oxygen-deficient $BiPO_4$ nanocubes.

It is well known that the reactive species $\bullet O^{2-}$, $h^+$ and •OH acted as a bridge, play the important roles in the photodegradation process of organic pollutants under the light irradiation. In order to investigate the possible mechanism that occurs on the oxygen-deficient $BiPO_4$ nanocubes the photodegradation experiments were carried out with p-benzoquinone, tert-butanol, and KI as scavengers for the reactive species of $\bullet O^{2-}$, •OH, and $h^+$, respectively. Figure 8 shows that the photodegradation of RhB was not suppressed in the presence of p-benzoquinone which may suggests that $\bullet O^{2-}$ was not the main active species in the degradation of the RhB. However, when the scavengers of •OH (tert-butanol) and $h^+$ (KI) were added into the solution, the photodegradation of RhB were significantly suppressed, which may suggested that •OH and $h^+$ played important roles in this photocatalytic reaction. Moreover, the •OH was investigated to have stronger inhibition effect than $h^+$ in this system.

In order to understand the photocatalytic mechanism occurring on the oxygen-deficient $BiPO_4$ nanocubes, it is necessary to calculate the conduction band (CB) and valence band (VB) of $BiPO_4$ because they played an important role in the photocatalytic oxidation process of organic molecule. Thus, the band edge positions of $BiPO_4$ were estimated in this study according to the following empirical formulas:[29]

$$E_{VB} = X - Ec + 0.5Eg \quad (3)$$

$$E_{CB} = E_{VB} - Eg \quad (4)$$

Where $E_{VB}$ is the valence band (VB) edge potential, $E_{CB}$ is the conduction band (CB) edge potential. Eg is the band gap energy of semiconductor which can be obtained from DRS (3.92 eV for $BiPO_4$) and Ec is the energy of free electrons on the hydrogen scale (about 4.5 eV). X is the electronegativity of the semiconductor, which is the geometric mean of the electronegativity of the constituent atoms (6.49

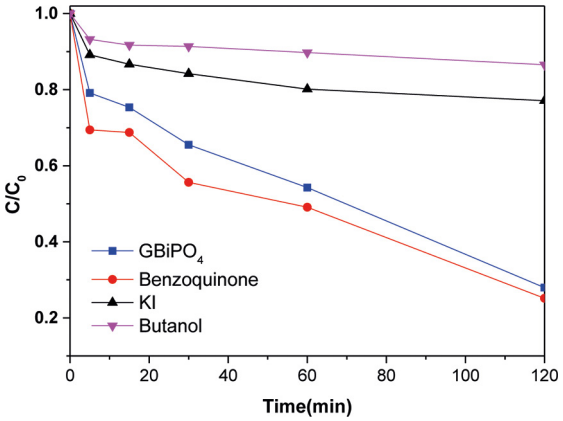


**Figure 8.** The influence of active species capturers on photocatalytic performance of $GBiPO_4$.

eV for $BiPO_4$). Based on the band gap positions, the $E_{VB}$ and $E_{CB}$ of BiPO4 were calculated to be 3.95 and 0.03 eV, respectively. The above results suggest that $BiPO_4$ has the higher valence band which can provide enough oxidation power of the holes.

The energy band structure diagram and possible mechanism of electron–hole separation and transportation at the $BiPO_4$ photocatalyst interface are illustrated in Figure 9. As can be investigated the pure $BiPO_4$ can not be excited under the visible light illumination due to its higher band gap. However, on the oxygen-deficient $BiPO_4$ nanocube photocatalyst, the generation of oxygen vacancy could result in the formation of the mid-gap states lying lower to the conduction band. The electrons can be excited up to oxygen vacancy states from the VB of $BiPO_4$ under visible light irradiation. Furthermore, the photo-induced electrons on oxygen vacancy states are not easy to recombine with photo induced holes as the oxygen vacancies are active electron traps. By trapping the active species during the photocatalytic reaction, •OH and $h^+$ were suggested as the main active species. Under visible light irradiation, electrons were excited to oxygen vacancy states and could produce •OH through a photogenerated electron-induced multistep reduction route. Photogenerated

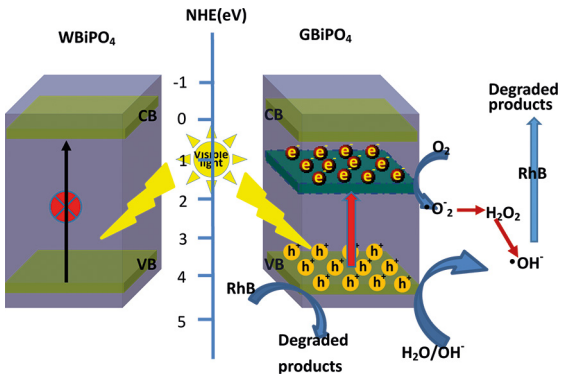


**Figure 9.** Schematic illustration of the charge separation and transfer in the $GBiPO_4$ photocatalysts under visible-light irradiation.

holes can oxidize RhB directly due to higher valence band of $BiPO_4$ and could also react with $OH^-$ to form •OH. Therefore, the oxygen vacancies in the oxygen-deficient $BiPO_4$ nanocubes can not only result in the enhancement of the separation efficiency of photoinduced electron–hole pairs but also expand the photoresponse range by forming the mid-gap states.

## 4. Conclusions

In summary, surface oxygen-deficient $BiPO_4$ nanocubes were synthesized by a hydrothermal process and subsequently an ultrasonic assistant Fe reduction process. The HRTEM and XPS results suggested that the oxygen vacancies were introduced on the surface of the $BiPO_4$ nanocubes. The surface oxygen-deficient $BiPO_4$ nanocubes showed greatly enhanced visible light induced photocatalytic activities. The enhancement of the photocurrent and photocatalytic performance and expanding of the photoresponse wavelength range were analytically due to the formation of mid-gap states lying lower to the conduction band of $BiPO_4$. This surface oxygen-deficient $BiPO_4$ nanocubes photocatalyst may provide new insights into the fabrication of photocatalysts with highly visible light induced photocatalytic performance.

## 5. Acknowledgment

This work is financially supported by National Nature Science Foundation of Zhejiang Province (No. LY12B07001).

## 6. References

1. Fujishima A, Honda K. Electrochemical Photolysis of Water at a Semiconductor Electrode. *Nature*. 1972;238:37-38.

2. Muñoz-Batista MJ, Fernández-García M, Kubacka A. Promotion of $CeO_2$–$TiO_2$ photoactivity by g-$C_3N_4$: Ultraviolet and visible light elimination of toluene. *Applied Catalysis B: Environmental*. 2015;164:261-270.

3. Fontelles-Carceller O, Muñoz-Batista MJ, Fernández-García M, Kubacka A. Interface Effects in Sunlight-Driven Ag/g-$C_3N_4$ Composite Catalysts: Study of the Toluene Photodegradation Quantum Efficiency. *ACS Applied Materials & Interfaces*. 2016;8(4):2617-2627.

4. Mohaghegh N, Tasviri M, Rahimi E, Gholami MR. A novel p–n junction $Ag_3PO_4$/$BiPO_4$-based stabilized Pickering emulsion for highly efficient photocatalysis. *RSC Advances*. 2015;5:12944-12955.

5. Zhang W, Jia B, Wang Q, Dionysiou D. Visible-light sensitization of $TiO_2$ photocatalysts via wet chemical N-doping for the degradation of dissolved organic compounds in wastewater treatment: a review. *Journal of Nanoparticle Research*. 2015;17(5):221.

6. Iliev V, Tomova D, Eliyas A, Rakovsky S, Anachkov M, Petrov P. Enhancement of the activity of $TiO_2$-based photocatalysts: a review. *Bulgarian Chemical Communications*. 2015;47(Special Issue C):5-11.

7. Yu H, Irie H, Hashimoto K. Conduction Band Energy Level Control of Titanium Dioxide: Toward an Efficient Visible-Light-Sensitive Photocatalyst. *Journal of the American Chemical Society*. 2010;132(20):6898-6899.

8. Dong S, Feng J, Fan M, Pi Y, Hu L, Han X, et al. Recent developments in heterogeneous photocatalytic water treatment using visible light-responsive photocatalysts: a review. *RSC Advances*. 2015;5:14610-14630.

9. Pan C, Zhu Y. New Type of BiPO4 Oxy-Acid Salt Photocatalyst with High Photocatalytic Activity on Degradation of Dye. *Environmental Science & Technology*. 2010;44(14):5570-5574.

10. Pan C, Zhu Y. A review of BiPO4, a highly efficient oxyacid-type photocatalyst, used for environmental applications. *Catalysis Science & Technology*. 2015;5:3071-3083.

11. She L, Tan G, Ren H, Xu C, Zhao C, Xia A. BiPO4@glucose-based C core–shell nanorod heterojunction photocatalyst with enhanced photocatalytic activity. *Journal of Alloys and Compounds*. 2016;662:220-231.

12. Chen D, Kuang Z, Zhu Q, Du Y, Zhu H. Synthesis and characterization of CdS/BiPO4 heterojunction photocatalyst. *Materials Research Bulletin*. 2015;66:262-267.

13. Liu L, Yao W, Liu D, Zong R, Zhang M, X. Ma X, et al. Enhancement of visible light mineralization ability and photocatalytic activity of $BiPO_4$/BiOI. *Applied Catalysis B: Environmental*. 2015;163:547-553.

14. Lin H, Ye H, Xu B, Cao J, Chen S. $Ag_3PO_4$ quantum dot sensitized $BiPO_4$: A novel p–n junction $Ag_3PO_4$/$BiPO_4$ with enhanced visible-light photocatalytic activity. *Catalysis Communications*. 2013;37:55-59.

15. Yin HY, Wang XL, Wang L, Lin Q, Zhao HT. Self-doped $TiO_2$ hierarchical hollow spheres with enhanced visible-light photocatalytic activity. *Journal of Alloys and Compounds*. 2015;640:68-74.

16. Henkel B, Neubert T, Zabel S, Lamprecht C, Selhuber-Unkel C, Rätzke K, et al. Photocatalytic properties of titania thin films prepared by sputtering versus evaporation and aging of induced oxygen vacancy defects. *Applied Catalysis B: Environmental*. 2016;180:362-371.

17. Ye L, Deng K, Xu F, Tian L, Peng T, Zan L. Increasing visible-light absorption for photocatalysis with black BiOCl. *Physical Chemistry Chemical Physics*. 2012;14:82-85.

18. Lv Y, Zhu Y, Zhu Y. Enhanced Photocatalytic Performance for the BiPO4–x Nanorod Induced by Surface Oxygen Vacancy. *Journal of Physical Chemistry C*. 2013;117(36):18520-18528.

19. Lv Y, Liu Y, Zhu Y, Zhu Y. Surface oxygen vacancy induced photocatalytic performance enhancement of a $BiPO_4$ nanorod. *Journal of Materials Chemistry A*. 2014;2:1174-1182.

20. Lin H, Ye H, Chen S, Chen Y. One-pot hydrothermal synthesis of $BiPO_4$/$BiVO_4$ with enhanced visible-light photocatalytic activities for methylene blue degradation. *RSC Advances*. 2014;4:10968-10974.

21. Weng S, Hu J, Lu M, Ye X, Pei Z, Huang M, et al. In situ photogenerated defects on surface-complex BiOCl (0 1 0) with high visible-light photocatalytic activity: A probe to disclose the charge transfer in BiOCl (0 1 0)/surface-complex system. *Applied Catalysis B: Environmental*. 2015;163:205-213.

22. Ye L, Jin X, Leng Y, Su Y, Xie H, Liu C. Synthesis of black ultrathin BiOCl nanosheets for efficient photocatalytic $H_2$ production under visible light irradiation. *Journal of Power Sources*. 2015;293:409-415.

23. Jiang J, Zhang L, Li H, He W, Yin JJ. Self-doping and surface plasmon modification induced visible light photocatalysis of BiOCl. *Nanoscale*. 2013;5:10573-10581.

24. Chen X, Liu L, Yu PY, Mao SS. Increasing solar absorption for photocatalysis with black hydrogenated titanium dioxide nanocrystals. *Science*. 2011;331(6018):746-750.

25. Wei Z, Liu Y, Wang J, Zong R, Yao W, Wang J, et al. Controlled synthesis of a highly dispersed $BiPO_4$ photocatalyst with surface oxygen vacancies. *Nanoscale*. 2015;7:13943-13950.

26. Li G, Ding Y, Zhang Y, Lu Z, Sun H, Chen R. Microwave synthesis of $BiPO_4$ nanostructures and their morphology-dependent photocatalytic performances. *Journal of Colloid and Interface Science*. 2011;363(2):497-503.

27. Xu J, Li L, Guo C, Zhang Y, Meng W. Photocatalytic degradation of carbamazepine by tailored $BiPO_4$: efficiency, intermediates and pathway. *Applied Catalysis B: Environmental*. 2013;130-131:285-292.

28. Liu H, Cheng S, Wu M, Wu H, Zhang J, Li W, et al. Photoelectrocatalytic Degradation of Sulfosalicylic Acid and Its Electrochemical Impedance Spectroscopy Investigation. *The Journal of Physical Chemistry A*. 2000;104(30):7016-7020.

29. Ye H, Lin H, Cao J, Chen S, Chen Y. Enhanced visible light photocatalytic activity and mechanism of $BiPO_4$ nanorods modified with AgI nanoparticles. *Journal of Molecular Catalysis A: Chemical*. 2015;397:85-92.